Supplementary Materials

The modelling of the electric-hydrogen coupling AC-DC hybrid microgrid together with the control method proposed in the paper "Fault-resilient Coordinated Voltage Control of Electric-Hydrogen Hybrid Microgrids with Battery-Fuel Cell Synergy" were implemented in Matlab/Simulink.

The microgrid model is mainly comprised of six parts. Figure S1 shows simulation modules of photovoltaic (PV) panels. PV panels are regulated by the maximum power point tracking (MPPT).

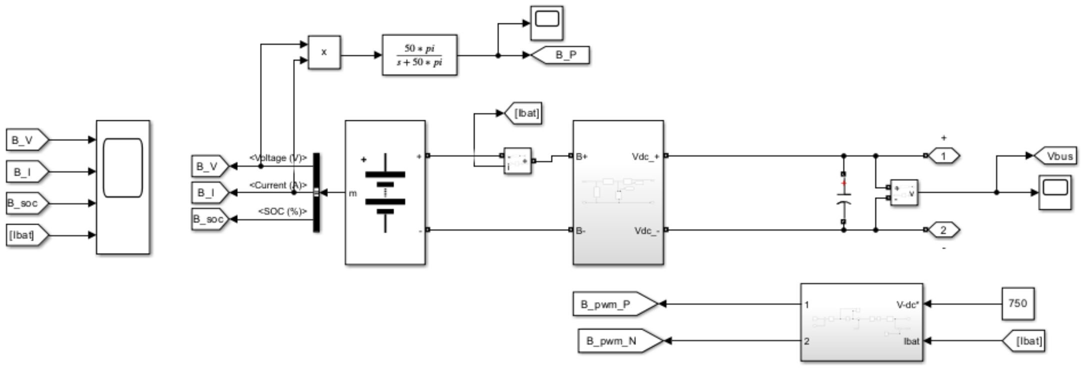

Figure S1. Simulation modules of PV panels within microgrid.

Figure S2 shows simulation modules of the battery energy storage system (BESS) connected to DC bus of the microgrid.

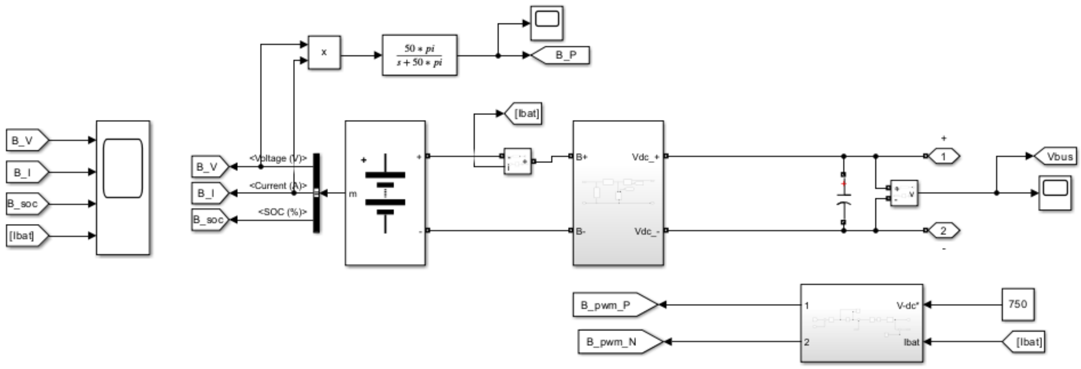

Figure S2. Simulation modules of BESS within microgrid.

Figure S3 shows simulation modules of electrolyser and hydrogen storage tank, including the U-I characteristic curve, hydrogen production rate and constant power control of EL, as well as HST pressure calculation.

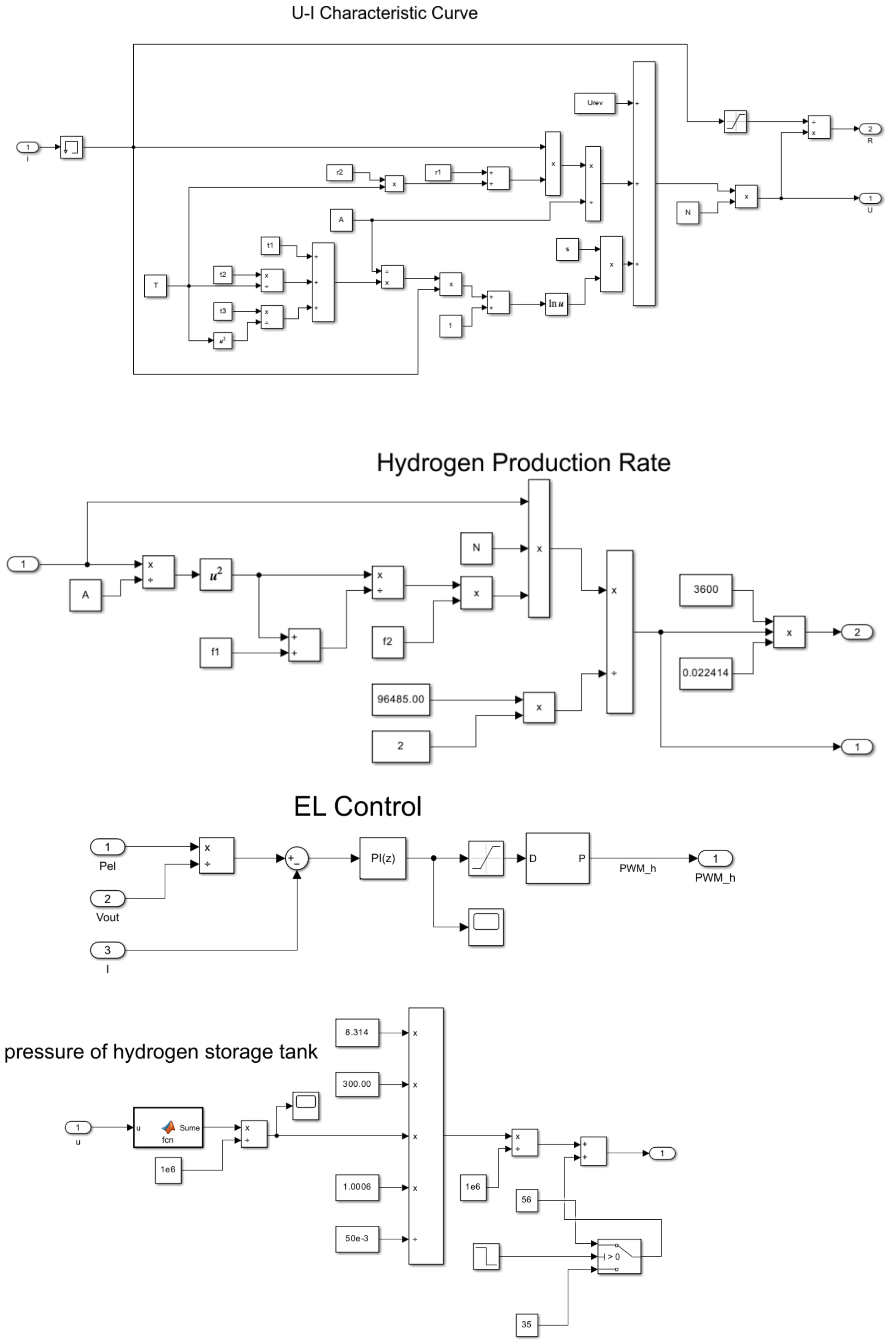

Figure S3. Simulation modules of electrolyser and hydrogen storage tank within microgrid.

Figure S4 shows simulation modules of virtual synchronous generator (VSG) control applied to a master converter. The VSG control comprises active power-frequency (P-f) control, reactive power-voltage (Q-V) control and virtual impedance control.

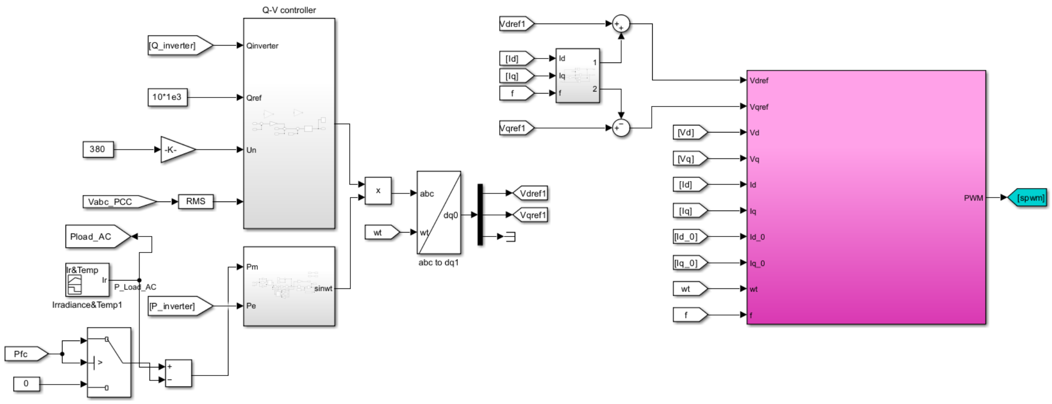

Figure S4. Simulation modules of VSG control of master converter.

To further demonstrate the innovative value of the proposed PI+PADRC, a comparison with a state-of-the-art advanced control algorithm, Finite Control Set Model Predictive Control (FCS-MPC), is provided in this section. The outer voltage loop retains the identical PI controller used in the main manuscript to ensure a fair comparison, while the inner current loop is replaced by the FCS-MPC. Euler method is adopted to perform multi-step prediction on the inductor current, which is given as follows:

$$i_{bat}(k+1) = i_{bat}(k) + \frac{T_s}{L}[U_{bat}(k) - s(k)U_{dc}(k)]\ s(k) \in \{0,1\}$$

To mitigate the effect of the digital control delay, the current at instant $k+1$ is first estimated using the switching state s_{prev} that was actually applied in the previous control period:

$$i_{bat}^{comp}(k+1) = i_{bat}(k) + \frac{T_s}{L}[U_{bat}(k) - s_{\text{prev}}U_{dc}(k)]$$

Starting from this compensated value, a two-step forward prediction is executed for each candidate switching state s_{i} (which, together with the initial compensation step, constitutes a total three-step prediction horizon):

$$i_{bat}^{(1)} = i_{bat}^{comp}(k+1) + \frac{T_s}{L}[U_{bat}(k) - s_{\text{i}}U_{dc}(k)]$$

$$i_{bat}^{(2)} = i_{bat}^{(1)} + \frac{T_s}{L}[U_{bat}(k) - s_{\text{i}}U_{dc}(k)]$$

where the future voltages are assumed constant over the prediction horizon.

The cost function is designed to minimize the absolute tracking error at instant $k+3$:

$$g(i) = \left|i_{\text{ref}} - i_{\text{bat}}^{(2)}\right|, \quad s_{\text{opt}} = argmin\, g(i)$$

The FCS-MPC scheme used in our Supplementary Materials was implemented exactly according to the method described in the paper: "Voltage Dynamic Response Optimization of DC Microgrid Based on Model Predictive Control" (Zhu et al., Power System Technology, Vol. 44, No. 6, 2020 DOI:10.13335/j.1000-3673.pst.2019.2071). In that reference:

A prediction horizon of three steps is explicitly adopted and validated as an effective trade-off between control performance and computational burden.

The cost function is defined as the absolute tracking error of the inductor current after three-step prediction, without additional weighting factors.

We directly inherited this design without modification, ensuring that our benchmark is not an arbitrary or crippled implementation, but rather a faithful reproduction of a published state-of-the-art method. The prediction horizon (N=3) and cost function structure are exactly as proposed in the reference.

Scenario I with Low SOC and High SOHC

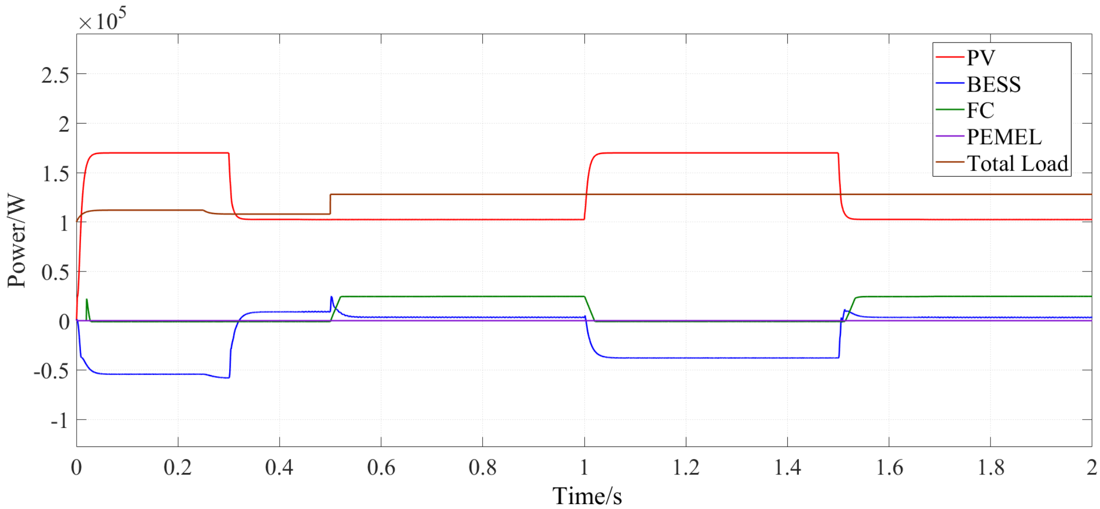

Figure S5. Power dynamics of microgrid components in Scenario I under the PI+FCS-MPC.

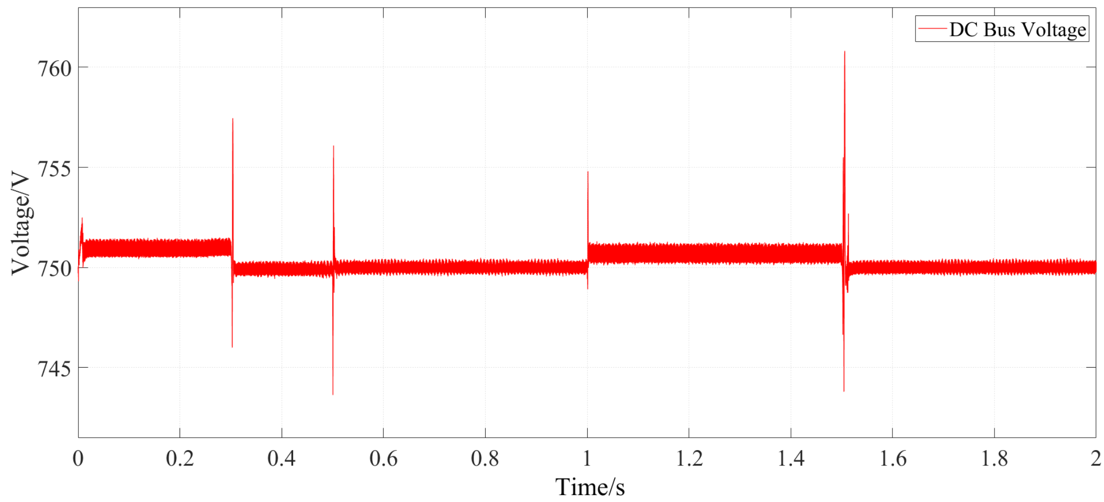

Figure S6. Dynamics of DC bus voltage in Scenario I under the PI+FCS-MPC.

Table S1. DC bus voltage fluctuation ranges in Scenario I under the PI+FCS-MPC.

Disturbance Time/s	Control Scheme	Bus voltage fluctuation range/V
0.3	PI+FCS-MPC	746~757.4
0.5	PI+FCS-MPC	744.3~768.1
1.0	PI+FCS-MPC	749.0~754.8
1.5	PI+FCS-MPC	743.8~760.8

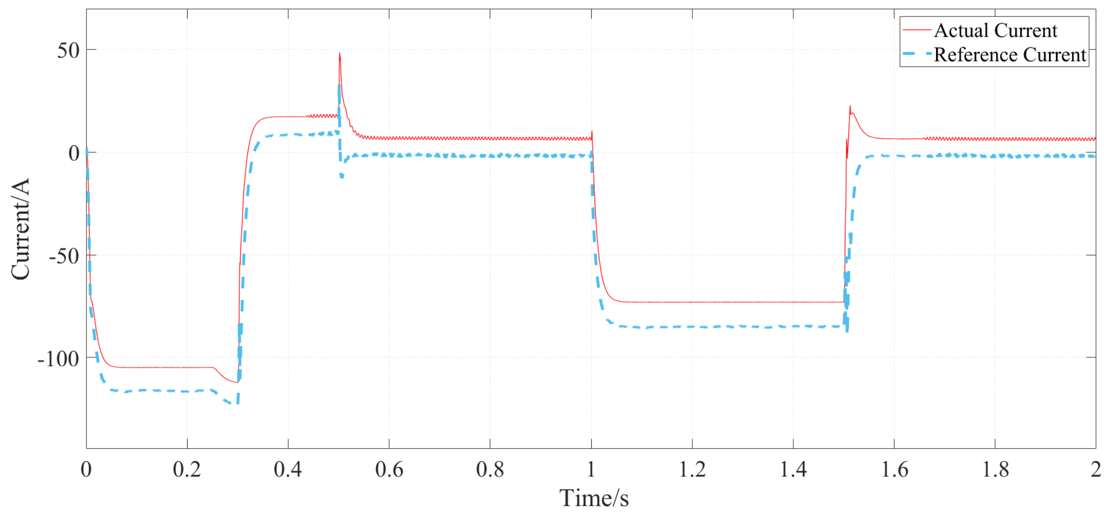

Figure S7. Dynamics of inductor current tracking in Scenario I under the PI+FCS-MPC.

As shown in the simulation results (Figure S7-S9), under minor load fluctuations, the proposed PI+PADRC demonstrates superior steady-state precision:

At t = 0.3 s, the PI+PADRC limits the voltage fluctuation to 4.8 V (746.9 V–751.7 V), which is significantly smaller than the PI+PI and PI+LADRC.

Notably, the PI+FCS-MPC exhibits a fluctuation range of 11.4 V, which is nearly double that of the proposed method. This indicates that the predictive control's sensitivity to model errors or noise leads to larger voltage ripples even under small disturbances.

At t = 1.0 s, a similar trend is observed. The PI+PADRC maintains a tight fluctuation range of 4.2 V (748.8 V–753.0 V), outperforming the PI+FCS-MPC (5.8 V).

When a severe power imbalance occurs at t = 0.5 s, the differences become more pronounced.

The PI+FCS-MPC suffers from the largest voltage fluctuation of 23.8 V, indicating a lack of sufficient damping during large transients.

The conventional PI+PI and PI+LADRC show fluctuation ranges of 20.0 V and 17.2 V, respectively.

In contrast, the proposed PI+PADRC restricts the fluctuation to only 14.1 V, demonstrating the most effective disturbance rejection capability.

Furthermore, regarding current tracking (Figure S9), the PI+FCS-MPC shows a noticeable current overshoot during the transient state, whereas the PI+PADRC achieves a smoother tracking response with effectively suppressed overshoot due to its nonlinear damping mechanism.

Scenario II with High SOC and Low SOHC

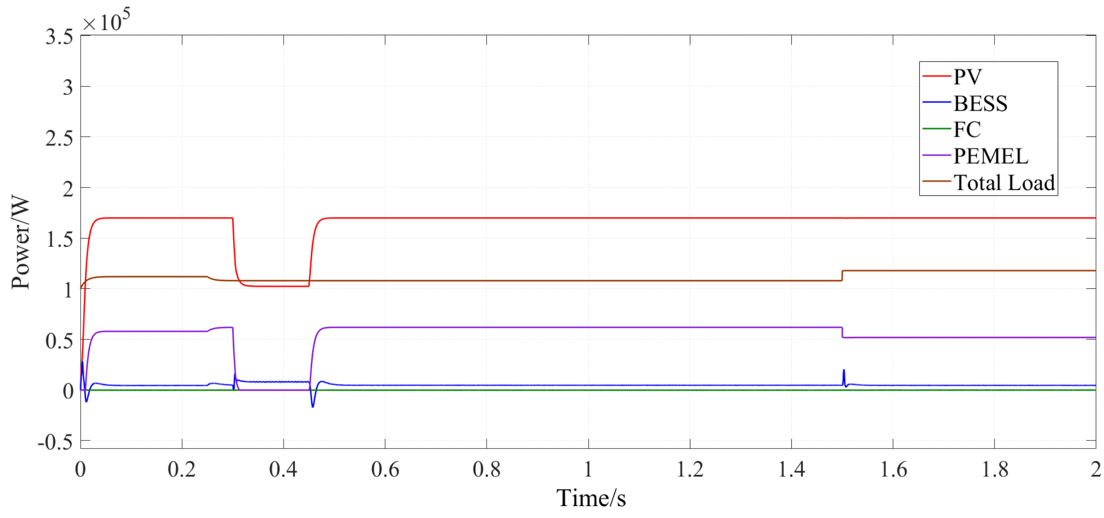

Figure S8. Power dynamics of microgrid components in Scenario II under the PI+FCS-MPC.

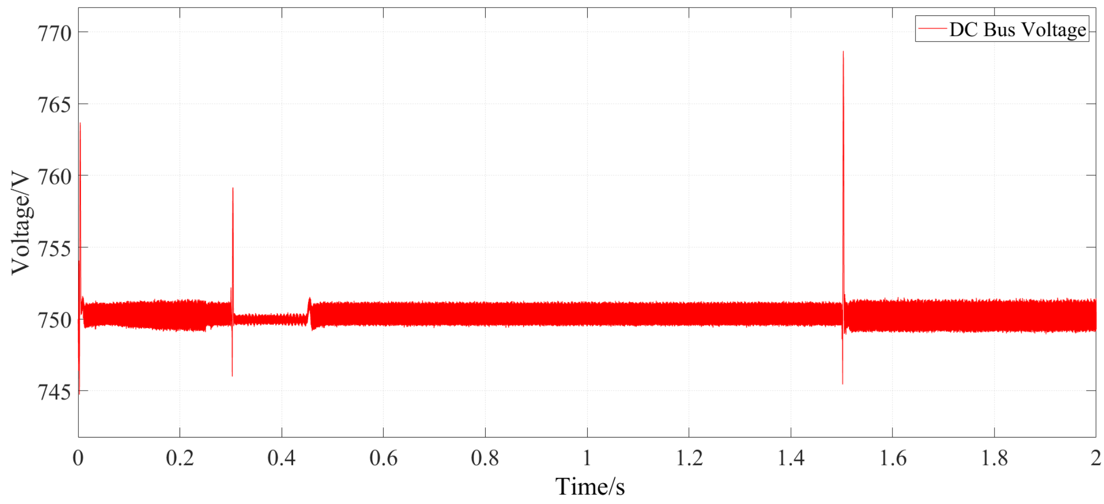

Figure S9. Dynamics of DC bus voltage in Scenario II under the PI+FCS-MPC.

Table S2. DC bus voltage fluctuation ranges in Scenario II under the PI+FCS-MPC.

Disturbance Time/s	**Control Scheme**	**Bus voltage fluctuation range/V**
0.3	PI+FCS-MPC	746.2~759.1
0.45	PI+FCS-MPC	749.0~751.5
1.5	PI+FCS-MPC	745.7~768.7

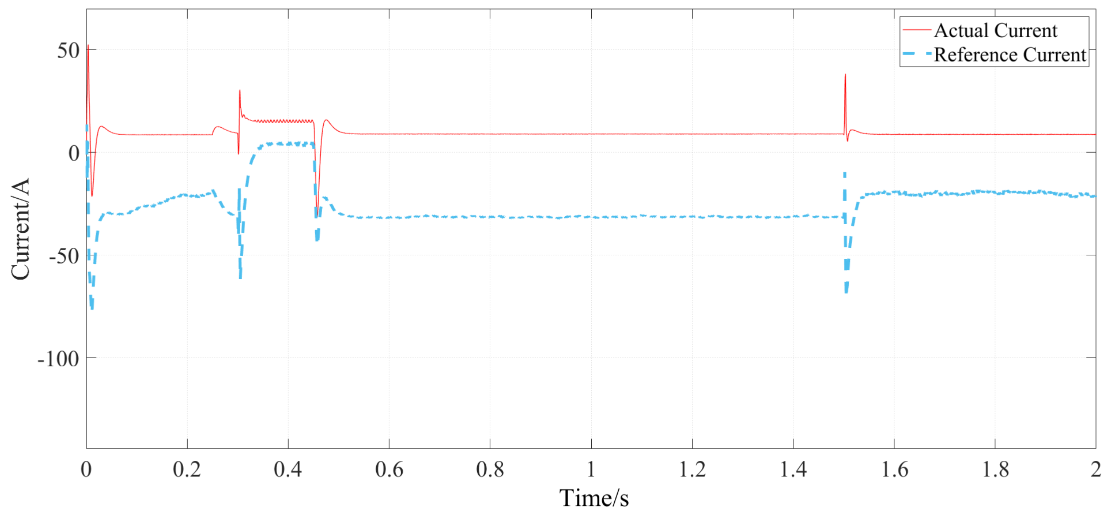

Figure S10. Dynamics of inductor current tracking in Scenario II under the PI+FCS-MPC.

As shown in the simulation results (Figure S10-S12), at t = 0.3 s, the PI+PADRC achieves a fluctuation range of 4.9 V.

The PI+FCS-MPC shows a fluctuation of 12.9V, again performing worse than the proposed method in terms of voltage stability.

At the minor step at t = 0.45 s, the PI+PADRC keeps the voltage within a 3V band, matching the performance of the FCS-MPC but with a smoother transient profile as seen in the current waveforms.

Under the large load increase at t =1.5s, the PI+FCS-MPC again exhibits the poorest performance with a massive fluctuation of 13 V.

The PI+PI and PI+LADRC controllers limit the fluctuation to 18.0 V and 5.5 V, respectively.

The proposed PI+PADRC achieves the best result, limiting the voltage deviation to just 4.8 V.

In terms of current tracking, the PI+FCS-MPC demonstrates the faster dynamic response than the PI+PI, with the actual current converging to the reference value.

In a word, the PI+FCS-MPC excels in current tracking speed but compromises DC bus voltage stability, especially under large disturbances. The proposed PI+PADRC successfully overcomes this limitation, delivering the most balanced performance by achieving the minimum voltage fluctuation and a fast, smooth current dynamic response in all tested scenarios.

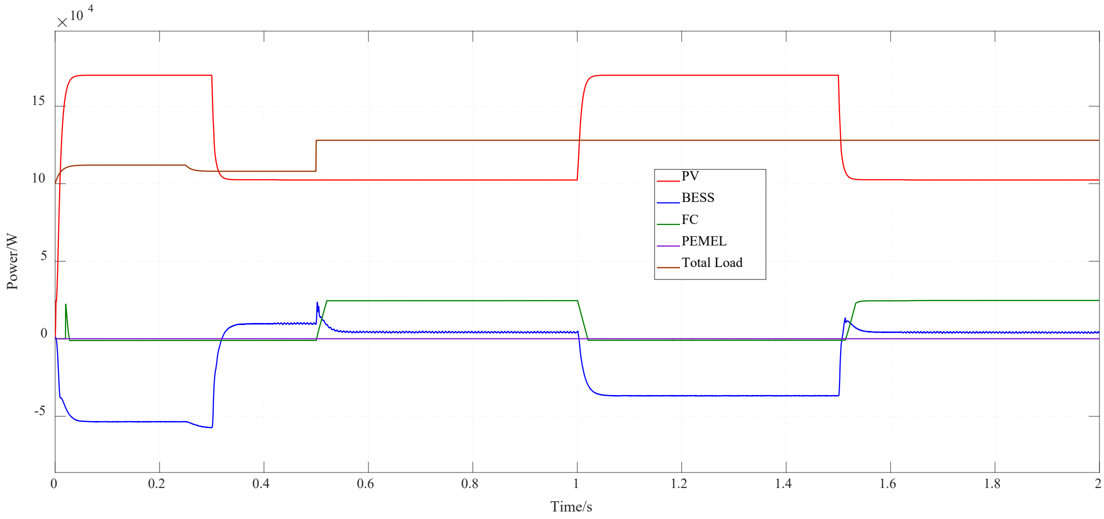

Figure S11. Power dynamics of microgrid components with noise injection into the inductive loop in Scenario I.